CONF-960982--5

UCRL-JC-123069

Fabry-Perot Measurements and Analysis of TOW-2A Liner Collapse and Jet Formation

S. C. Simonson, K. A. Winer, R. D. Breithaupt,
G. R. Avara, D. W. Baum

This paper was prepared for submittal to the
16th International Symposium on BALLISTICS
San Francisco, CA
September 23-28, 1996

July 1996

Lawrence Livermore National Laboratory

16TH INTERNATIONAL SYMPOSIUM ON BALLISTICS
SAN FRANCISCO, CA, 23-28 SEPTEMBER, 1996

FABRY-PEROT MEASUREMENTS AND ANALYSIS OF TOW-2A LINER COLLAPSE AND JET FORMATION

S. Christian Simonson, Kris A. Winer, R. Don Breithaupt,
G. Rex Avara, and Dennis W. Baum

Lawrence Livermore National Laboratory, P.O. Box 808 L-170
Livermore, CA 94551-0808 USA

A TOW-2A 146-mm shaped charge was fired and observed with five-beam Fabry-Perot laser velocimetry. The liner collapse velocities were measured at five lines of sight covering the outer half of the liner. A record of 8-10 μs in length was obtained for each sight line. The velocity records at late time differ for each location, reflecting the varying charge-to-mass ratio as the end of the liner is approached. The results were analyzed with the CALE 2-D hydrodynamic simulation code. The calculations reproduce the jump-off times, the shapes of the velocity jumps, and the late-time velocity asymptotes, but they underestimate the jump-off velocities by 6-7%. The calculations show that there exist no features in the velocity records that require spallation to account for them. Rather, the standard Steinberg-Guinan material model adequately accounts for the response of this copper liner to LX-14.

INTRODUCTION

As part of an effort to obtain better information on the behavior of liner materials in shaped charges, an experiment was conducted to observe the liner collapse process by means of multi-beam Fabry-Perot velocimetry [1]. The time resolution of the Fabry-Perot velocimeter is high enough to see the important features of the liner acceleration after the passage of the detonation wave in the high explosive (HE). By employing multiple beams, the effect of varying charge-to-mass (C/M) ratio along the liner can be studied.

An additional reason for studying the liner acceleration is to observe or infer the pattern of density waves in the liner as it collapses. When these density waves arrive in the convergence zone, they cause oscillations in the pressure that drives the jet (see, for example, [2]). Depending on the magnitude and frequency of these pressure oscillations in the convergence region, it is conceivable that they could influence the eventual breakup of the jet. If the wave pattern were the result of a simple process of shock propagation and reverberation in a homogeneous liner, then the amplitude of the density waves may remain fairly large during the collapse process, and one might expect a series of regular pressure oscillations in the convergence region. If, on the other hand, an internal spall surface were to develop, with wave reflections off interior and exterior boundaries, plus the generation of additional waves when the spall layer closes, then these multiple waves reverberating in the liner would lead to a complicated pattern of pressure oscillations in the jet formation region. For these reasons, the Fabry-Perot measurements may have implications for eventual jet particulation as well as for liner collapse.

EXPERIMENT

A TOW-2A shaped charge was used in the experiment. Its relatively large 146-mm charge diameter provided a convenient scale for placing multiple beams along the liner. The TOW-2A has a biconic liner of copper. In the region where the beams were placed, the liner has a constant angle and uniform thickness. The full angle is specified to be 42°, and the thickness is specified to be 2.29 +0.00/-0.15 mm. No measurements were made of the actual liner fired. The main charge is LX-14, and it was fired uncased with an equivalent of the TOW-2A precision initiation coupler and an RP-2 detonator.

Five Fabry-Perot beams were used, which were placed at 20-mm intervals along the liner, starting at 10 mm from the base of the liner, as shown in Figure 1. The beams were all in a plane which passed through the axis of symmetry and which was perpendicular to the inside surface of the liner. The nominal angle of the beams from the face of the charge was intended to be 67°, or 46° from the surface of the liner. In order to accommodate the dimensions of the Fabry-Perot probes while maintaining the 20-mm interval, the angles of the beams were all slightly different, as noted in Figure 1. The time domain of the velocity measurements began at surface jump-off and continued for approximately 10 μs. The Fabry-Perot records for the five cameras are reproduced in Figure 1.

VELOCIMETRY RESULTS

From each Fabry-Perot record, a line-of-sight velocity curve was generated. These are shown in Figure 2(a). As only a single cavity was employed, the Fabry-Perot records are uncertain by a multiple of the fringe constant, 0.61 km/s. This ambiguity was resolved by comparison with continuum mechanics code calculations. The dynamic distortion in the electronic streak cameras was corrected prior to the analysis. Each record was corrected for delay times produced by electronic cables, fiber-optic cables, light velocity in air, and for fiducial light generation. The standard errors for the velocity curves are given as a function of time in Figure 2(b). Each error curve represents one standard deviation. Residuals have been calculated from the velocity curves as deviations from the theoretically required constancy of radius-squared differences between adjacent fringes and from the required symmetry of top to bottom fringes on a record.

Time uncertainties of a velocity record are dominated by the streak camera's slit width, which is 0.1 mm at the film. Time errors are calculated from residuals of the intervals between a record's time marks and by comparing top fiducials to bottom fiducials. Absolute time errors include 0.07 μs uncertainty of unresolved cable corrections. The results are an uncertainty of 0.03 km/s in velocity, 0.10 μs in absolute time, and 0.03 μs in relative time (i.e., between two cameras).

The velocity records at late time differ for each location, reflecting the varying charge-to-mass ratio as the end of the liner is approached. However, there is a high degree of consistency from one record to the next in the shapes of the early velocity steps. The detailed shapes will be discussed in connection with the continuum mechanics code calculations.

HYDRODYNAMIC MODEL

In order to better understand the features seen in the Fabry-Perot records, the experiment was modeled using the LLNL continuum mechanics simulation program, CALE [3]. CALE is an Arbitrary Lagrangian-Eulerian code, which makes it well suited for modeling a shaped charge such as the TOW-2A, since it allows the mesh to conform to the liner, which makes an acute angle with the axis of symmetry. We will first discuss the zoning and the material models, and then take up the calculational results.

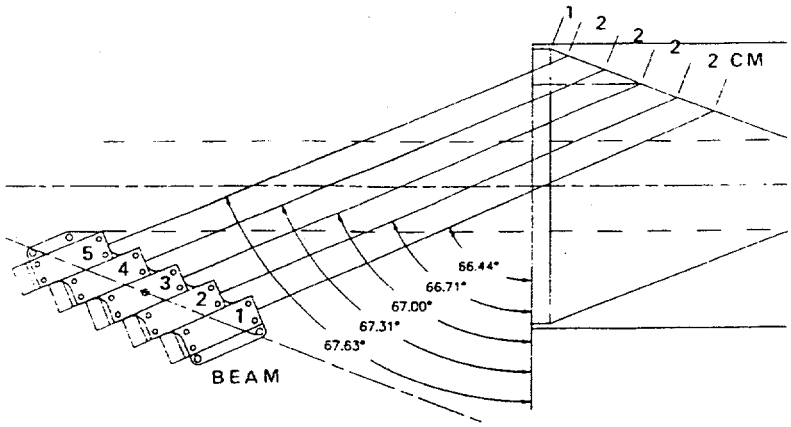

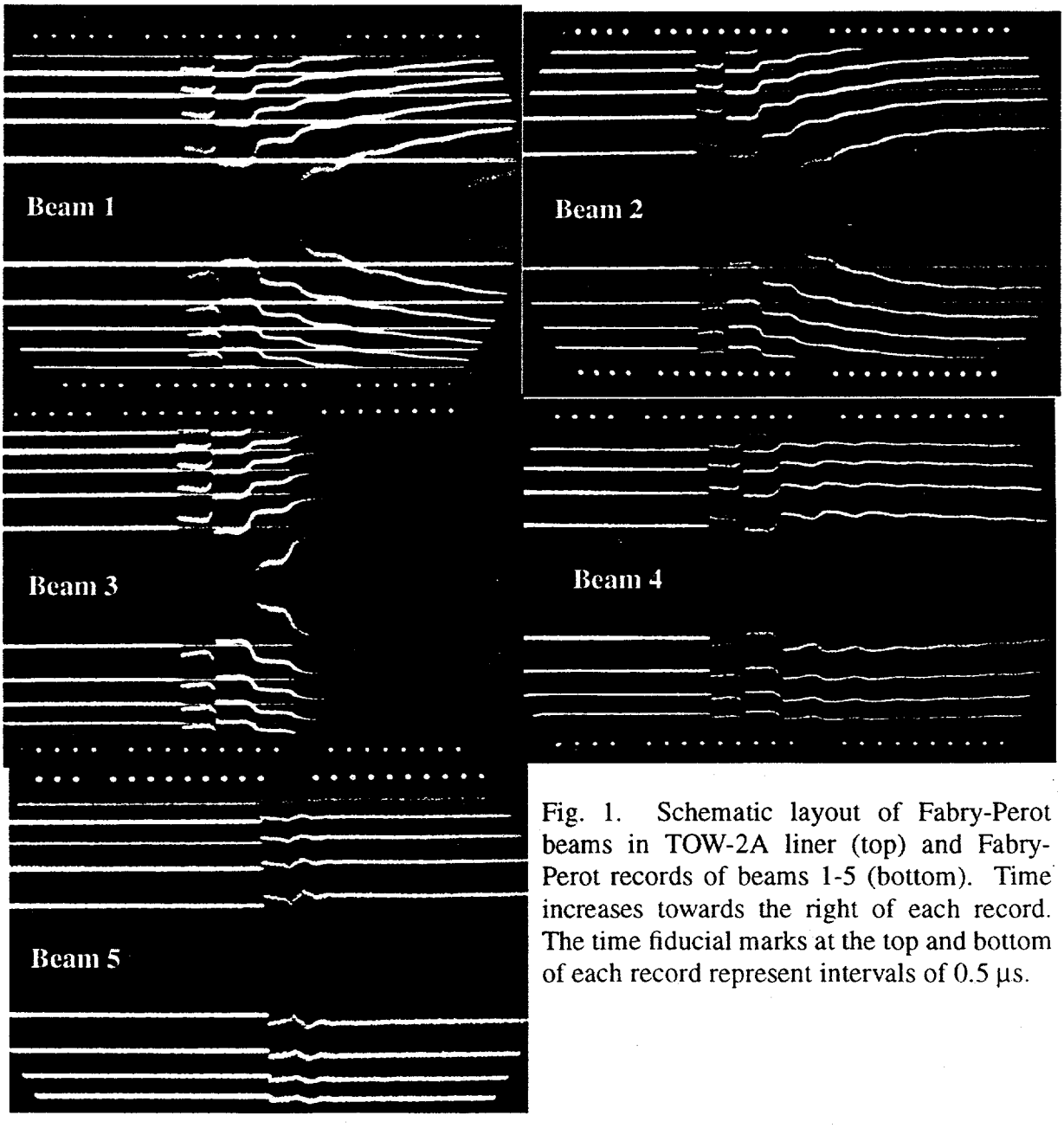

Fig. 1. Schematic layout of Fabry-Perot beams in TOW-2A liner (top) and Fabry-Perot records of beams 1-5 (bottom). Time increases towards the right of each record. The time fiducial marks at the top and bottom of each record represent intervals of 0.5 μs.

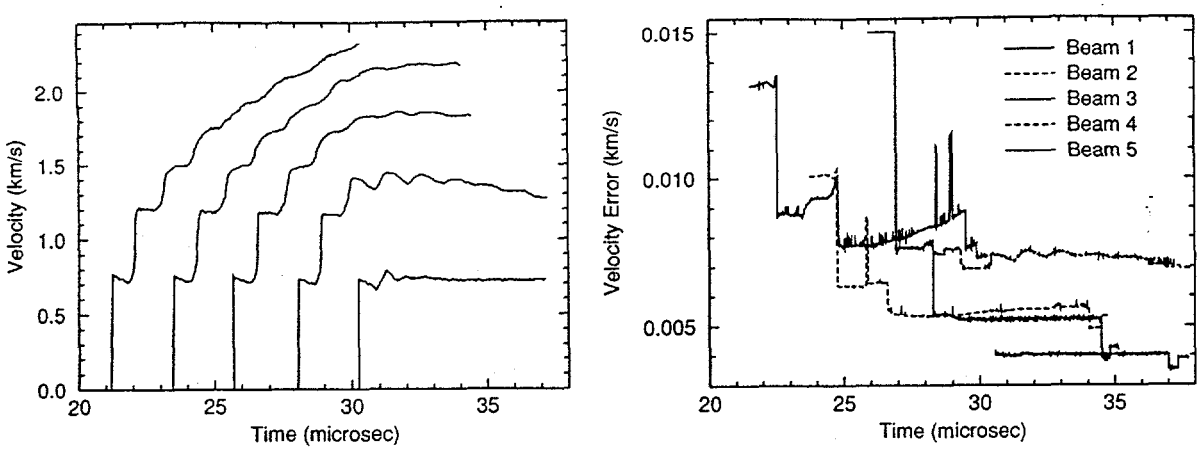

Fig. 2.—(a)Velocity curves for Fabry-Perot beams 1-5 (*left*). (b) Errors for Fabry-Perot velocities (*right*).

Zoning

The calculational mesh was set up to resolve wave motions along and across the liner with equivalent resolution in the time domain. The detonation wave sweeps along the liner at 8.9 km/s, while the shock travels across the liner at 6.4 km/s, roughly a 4:3 ratio. The mesh in the liner was constructed with rectangular zones in a 4:3 aspect ratio. This zoning was continued into the HE, except that one set of lines was tilted forward 8° in order to be more nearly aligned with the detonation front. Away from the locations of the Fabry-Perot beams, the mesh was gradually expanded to a larger size for calculational efficiency. As we are employing the program-burn model, the buildup of pressure in the detonation wave occurs over three zones. Thus the resolution is about one third of the number of zones. If one considers high resolution to consist in placing ten or more elements across the liner, one would need at least 30 zones to accomplish this. Medium resolution could be considered as having five elements across the liner, or 15 zones.

Material Models

The HE equation of state (EOS) used in these calculations is in the Jones-Wilkins-Lee (JWL) format [4]. Two separate formulations were used [5], one with a relatively high value of the Chapman-Jouget pressure (P_{CJ} = 38.1 GPa) and one with a lower value (P_{CJ} = 35.8 GPa). For the liner, the Steinberg-Guinan constitutive model [6] for half-hard OFHC copper was used. In order to model ductile failure, the minimum pressure was set to -1.2 GPa, with the pressure held at that value if it fell below it. The minimum relative density was set to 80%, and the maximum equivalent plastic strain was set to 2.0.

CALCULATIONAL RESULTS

Two sets of CALE calculations were made, one with medium resolution to model the first few reverberations of the shock in the liner, and one with low resolution to model late-time behavior.

Medium-Resolution Calculations

The medium-resolution calculation used 15 zones across the liner. The velocity as seen by the Fabry-Perot beam was constructed by projecting the beam until it encountered a zone containing liner material. A weighted average was then made of the velocities of the two corner nodes at the liner side of the zone, and this was projected onto the beam angle.

A diagram of the mesh and the first beam is shown in Figure 3(a), along with the pressure field. The corresponding density distribution is shown in Figure 3(b). As can be seen in Figure 3(a), the detonation wave in the HE is aligned with the mesh lines, and the buildup of pressure occupies about three zones. The shock in the liner is also spread over three zones in the longitudinal and transverse directions, and it occupies 15 zones along the liner and 15 zones across the liner, showing equivalent zone size in each dimension. Following the shock, the density distribution responds to the pressure field both from the reflected rarefaction wave and from the pressure in the HE behind the detonation front. As an example of this effect, the shape of the density distribution in Figure 3(b) is somewhat irregular at the lower left-hand edge, i.e., at the second maximum in the density wave.

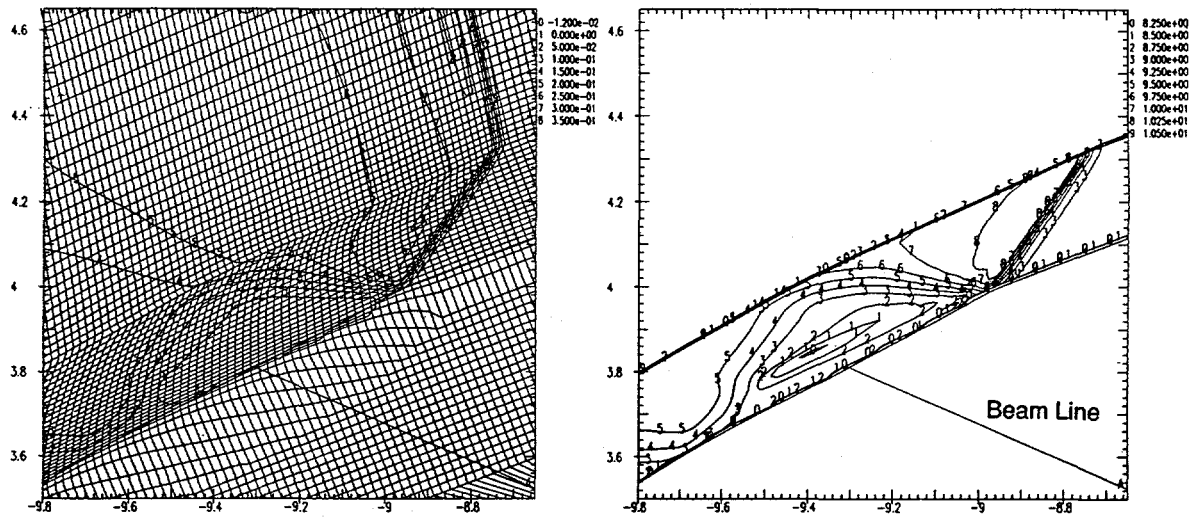

Fig. 3.—(a) CALE mesh in vicinity of first beam at 17 μs (21.7 μs experimental time), showing pressure field (*left*), and (b) corresponding density contours (*right*). Coordinates are given in centimeters, pressure contours in 100 GPa, density contours in g/cm^3.

A comparison of the results of the medium-resolution calculation with the Fabry-Perot data is shown in Figure 4(a) for the first three beams. The calculational results have been shifted by 4.7 μs to account for the detonation train function time. In the calculations, the first jump has a small double peak, which is partially an effect of the zoning and the velocity construction algorithm. The velocity then pulls back under the influence of the rarefaction tension, followed by the second step, the third step, etc.

The medium-resolution calculation used the 35.8-GPa EOS for the HE, and no modifications were made to the strength parameters for the copper. The minimum density ratio encountered by the calculations was about 92%, and the maximum equivalent plastic strain accumulated in each velocity jump was about 20%. Therefore, none of the failure thresholds was exceeded, and the copper retained its customary strength in the Steinberg-Guinan model.

The main difference between the calculated velocities and the measured velocities is that the calculated velocity jumps are about 6-7% greater in amplitude than the data, at least in the first two beams. This leads to a proportionately longer interval between velocity steps in the calculation, and the phase difference increases with each step.

If this phase difference is discounted, the shapes of the succeeding steps in each of the calculated beams are quite similar to those in the data. That is, in the first velocity step, the data

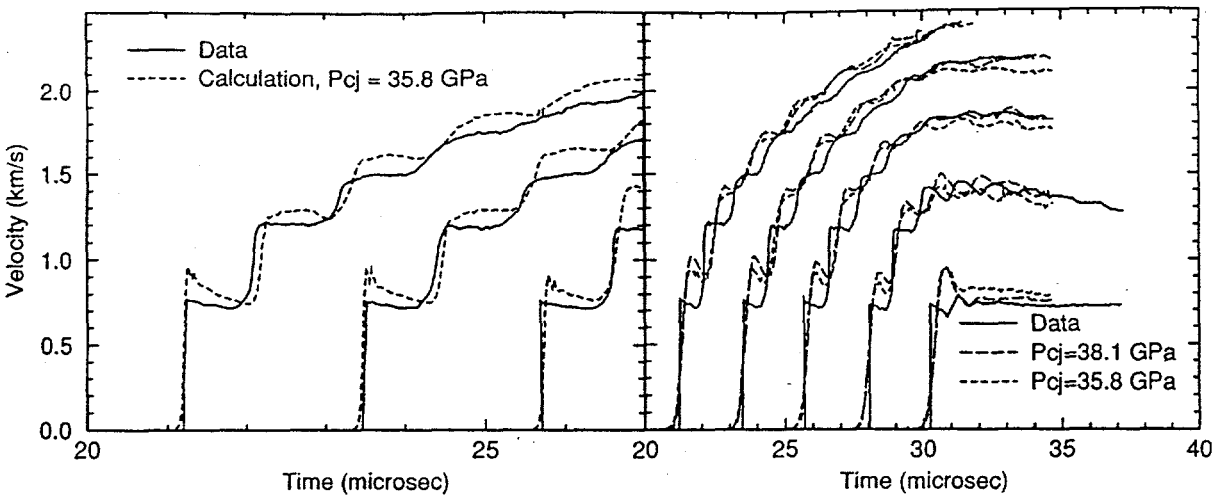

Fig. 4.—Results of CALE calculations, compared with data: (a) medium-resolution (*left*), (b) low-resolution(*right*).

show a pulling back from the initial jump, and the calculations show this also, but somewhat more exaggerated. In the second step, the data show a flat top, while the calculations in the first two beams are more rounded and in the third beam show some pulling back. In the third step, the data show a gradual rise and then a flat portion, which is represented closely by the calculations. In the fourth step, the data show a rounded hump, which is also closely represented by the calculations.

As the shapes of the features in the velocity data are represented in a qualitative sense by the calculations, differing primarily by a 6-7% change in amplitude with a corresponding phase shift in time, there is no reason to invoke spall surfaces or damage regions to account for any of the features seen in the data.

Low-Resolution Calculations

The low-resolution calculations were used to examine the late-time behavior of the liner. These calculations used ten zones across the liner, with a 6:1 aspect ratio for the zones along the liner. Thus the waves along the liner were covered by about 8-10 zones from one peak to the next. Two sets of JWL parameters for the HE EOS were used, as noted earlier.

The resulting velocity records are compared with the data in Figure 4(b). As with the medium-resolution calculation, these calculations produced larger-amplitude early-time velocity jumps than in the data, thus causing a progressive phase shift along the velocity record. However, unlike the medium-resolution calculations, the detailed shape of each jump is not well represented. At later times, the 38.1-GPa EOS gives a good match to the final velocity.

The data indicate that the varying C/M ratio along the liner has almost no effect on the initial jump-off, even for the last beam. The first four beams show no effect at the second velocity step, the first three beams show no effect at the fourth step, and the first two beams show no effect at the sixth step. It is only at later times that the decrease in available energy in the HE products from the decreasing C/M ratio becomes evident.

CONCLUSIONS

The multi-beam Fabry-Perot velocimetry technique is a useful technique for examining the material behavior of a shaped charge liner. It carries out what essentially amount to multiple

experiments simultaneously, so that the consistency among the results indicates the degree of reproducibility. In this case, the consistency was high. Thus there can be a reasonable degree of confidence that the details in the experimental record that vary from one velocity step to the next represent real features in the material behavior of the liner and the HE. These measurements can serve as a benchmark for detailed comparison with hydrodynamic simulation code calculations.

The calculations show that there exist no features in the velocity records that require spallation to account for them. Rather, the standard Steinberg-Guinan material model adequately accounts for the response of this copper liner to LX-14. The late-time expansion appears to be well characterized by a current JWL EOS. The EOS of the HE, however, may require further adjustment to the prompt energy delivery rate to remove the last 6-7% excess velocity for the initial jump-off.

From a comparison of the calculated and measured velocities, a regular pattern of waves appears to be present in this liner, modified only by the details of the pressure and density distributions. However, as shown by the detailed shapes of the velocity steps in the Fabry-Perot records, this pattern differs from that of a purely sinusoidal oscillation. Thus it will require calculations using at least medium resolution in the liner, carried all the way into the convergence zone, to explore the effects on jet formation and the possible implications for jet particulation.

ACKNOWLEDGMENTS

The authors wish to thank R. E. Tipton and L. C. Haselman for useful discussions regarding the hydrodynamic modeling. Lloyd Steinmetz, Richard Whipkey and Larry Booth contributed to the Fabry-Perot velocimetry. Work was performed under the auspices of the U.S. Department of Energy by Lawrence Livermore National Laboratory under contract No. W-7405-Eng-48. This work was supported in part by the Joint DoD/DOE Munitions Technology Development Program.

REFERENCES

1. McMillan, C. F., Goosman, D. R., Parker, N. L., Steinmetz, L. L., Chau, H. H., Huen, T., Whipkey, R. K., Perry, S. J. 1988, *Reviews of Scientific Instruments* **59**, 1.
2. Miller, S. 1995, *15th Int. Symp. on Ballistics*, Jerusalem, Israel, Vol. 2, p. 191.
3. Tipton, R. E. 1996, "CALE User's Manual", private communication.
4. Dobratz, B. M., and Crawford, P. C. 1985, *LLNL Explosives Handbook*, Lawrence Livermore National Laboratory, Livermore, CA, UCRL-52997.
5. Haselman, L. C. 1996, private communication.
6. Steinberg, D. J., Cochran, S. G., Guinan, M. W. 1980, *J. Applied Physics* **51**, 1498.